

Evolution of Intermetallic Phases in Soldering of the Die Casting of Aluminum Alloys



JIE SONG, XIAOMING WANG, TONY DENOUDEN, and QINGYOU HAN

Most die failures are resulted from chemical reactions of dies and molten aluminum in the die casting of aluminum. The formation of intermetallic phases between a steel die and molten aluminum is investigated by stationary immersion tests and compared to a real die casting process. Three intermetallic phases are identified in the stationary immersion tests: a composite layer and two compact layers. The composite layer is a mixture of α_{bcc} , Al, and Si phases. The α_{bcc} phase changes in morphology from rod-like to spherical shape, while the growth rate of the layer changes from parabolic to linear pattern with immersion time. The first compact layer forms rapidly after immersion and maintains a relatively constant thickness. The second compact layer forms after 4 hours of immersion and exhibits parabolic growth with immersion time. In comparison, only a composite layer and the first compact layer are observed in a real die casting process. The fresh molten aluminum of high growth rate washes away the second intermetallic layer easily.

DOI: 10.1007/s11661-016-3454-2

© The Minerals, Metals & Materials Society and ASM International 2016

I. INTRODUCTION

H13 dies are widely used in high pressure die casting (HPDC) of aluminum alloys due to its advantages in short production cycles, nearly net-shaped products, and highly efficient operations.^[1,2] A380 is an excellent die casting aluminum alloy at low cost, with good castability and mechanical properties.^[3] Die failure through soldering is one of the most important issues in HPDC of aluminum alloys. Die soldering mostly includes the following steps: (1) barrier failure between dies and casting alloys, (2) reactions between dies and molten aluminum alloys, and (3) solidified materials attaching to reaction areas. When soldering occurs, dimensions of the die cavity change due to the soldering product that remains in the die. The die surfaces need to be polished in order to remove the soldering product, leading to an increase of down time and cost. It is thus essential to address and prevent the formation of intermetallics between dies and casting alloys and the consequent soldering.^[3] Soldering starts from barrier failures including coating and lubricant failure which creates an opportunity for the reaction between the die material and molten alloy. When reactive die material and molten alloy are brought into contact, soldering

products are produced and attached to the surface of the die. To understand the chemical reaction and its intermetallic products in soldering, diffusion tests between iron and aluminum have been adopted.^[3–17] Furthermore, immersion tests of H13 tool steel into aluminum alloys have been conducted to understand the formation of intermetallic phases in industrial production.^[1,2,9,18–20]

According to diffusion theories, the product layer thickness initially follows a linear relation with time due to the chemical reaction nature at the beginning of immersion. The thickness increase then changes to parabolic with time after a thinner reaction layer formed when the diffusion controlled reaction process is dominated.^[11,12] The thickness of each phase layer depends on its growth rate, molar volume, and solubility as well as the consumption rate by other phases.^[10,17] The intermetallic phases in an Al-Fe binary diffusion couple are Al_5Fe_2 , AlFe, AlFe_3 , etc., dependent on various diffusion times, temperatures, and also trace elements.^[5,6] The interphase shows an irregular morphology with tongue-like shape in general.^[4,7,9,16] Temperature has a profound effect on the Al-Fe diffusion couple. Al_5Fe_2 can form at lower temperatures, while AlFe and AlFe_3 form at temperatures higher than 1273 K (1000 °C).^[6,7] Alloying elements may also play an important role in the reaction. Carbon in steel, for example, diffuses to the interface between the reaction layer and steel substrate through grain boundaries to form an Al_4C_3 phase. Al_4C_3 and C weaken the grain boundaries, leading to grain detachment from substrate.^[3] A small amount of Si and Mg elements retard diffusion rate of aluminum by building up at the interface and reducing the diffusion capability of aluminum.^[2,3] Intermetallic compounds produced through chemical reaction of H13 tool steel and an Al-11Si-3Cu alloy under 953 K (680 °C) and 5 hours in an immersion test were

JIE SONG, Formerly PhD Student with the School of Engineering Technology, Purdue University, 401 N. Grant St., W. Lafayette, IN 47907, is Postdoctoral Researcher with the Department of Metallurgical and Materials Engineering, Colorado School of Mines, 1500 Illinois St., Golden, CO 80401. Contact e-mail: j.song.thu@gmail.com XIAOMING WANG, Assistant Professor, and QINGYOU HAN, Professor, are with the School of Engineering Technology, Purdue University. TONY DENOUDEN, Engineer, is with Fiat Chrysler Automobiles, 800 Chrysler Drive, Auburn Hills, MI 48326.

Manuscript submitted August 3, 2015.

Article published online March 22, 2016

identified as cubic α_{bcc} (AlFeSiCrMnCu), hexagonal $\text{Al}_8\text{Fe}_2\text{Si}$, and orthorhombic Al_5Fe_2 .^[1] Large amount of Si and Cu elements also changed the interface from tongue-shape to flat.^[1,7] However, information about the transition of intermetallic phase under different durations, morphology of each intermetallic phase, diffusion mode between H13 and hypoeutectic commercial Al-Si alloy, and differences between immersion test and real HPDC is still not available.

In this study, stationary immersion test of H13 tool steel in molten A380 aluminum alloy at different time periods are performed to understand the formation of intermetallic phases, diffusion modes in each phase, and morphology changes with diffusion time. In order to compare the immersion testing results with a real HPDC process, samples in real HPDC are also analyzed.

II. EXPERIMENTAL METHODS

Tempered commercial H13 tool steel (HRC 45) and A380 aluminum alloy were used in the investigation. Their compositions are Fe-5.24 wt pct Cr-1.36 wt pct Mo-1.06 wt pct V-1.01 wt pct Si-0.35 wt pct C and Al-8.98 wt pct Si-3.71 wt pct Cu-1.39 wt pct Fe-3.05 wt pct Zn, respectively.

H13 tool steel samples of diameter 20 mm and height 5 mm were immersed in molten aluminum alloy for stationary immersion tests. The surface of H13 tool steel samples were ground to 600 grit, polished to 3 μm , and cleaned by ethanol under ultrasonic vibration. A

graphite crucible containing 1.5 kg molten aluminum alloy was heated in an electrical resistance furnace. A melting temperature was set to 1023 K (750 °C) to melt silicon in the alloy and then lowered to a temperature between 933 K and 938 K (660 °C and 665 °C). The entire process was closely monitored by using a k-type thermocouple. The immersion time varied from as short as 113 seconds to up to 64 hours (113 seconds, 0.0625, 0.125, 0.25, 0.5, 1, 2, 4, 8, 16, 32, and 64 hours). Immersion samples were quenched in water right after being taken out of molten aluminum to stop further reaction or diffusion, followed by sectioning through symmetrical axis for further analysis.

Core pins of 6 mm in diameter and 50 mm in length were used for real HPDC process, which was carried out on an Idra OL4000 3600 metric ton HPDC machine (Idra Presse S.P.A., Brescia, Italy). The casting temperature was chosen as 933 K (660 °C). A Chem-Trend 1699CK die release agent was used at a lube-to-water ratio of 1:70. After a severe soldering, the core pins were removed from the dies and were cut perpendicular to axial direction for microstructure analysis.

X-ray diffraction samples were taken from the cross section of stationary immersion samples and were ground to 600 grit. A Bruker general area diffraction detector was operated at 30 kV and 30 mA to determine phases of the soldering product. The source spot size was 0.8 mm in diameter with a chrome target ($K\alpha_1$: $\lambda = 2.2897 \text{ \AA}$) to reduce Fe fluorescence. A red laser and built-in microscope were assisted to locate the interesting areas with an accuracy of 100 μm . XRD patterns

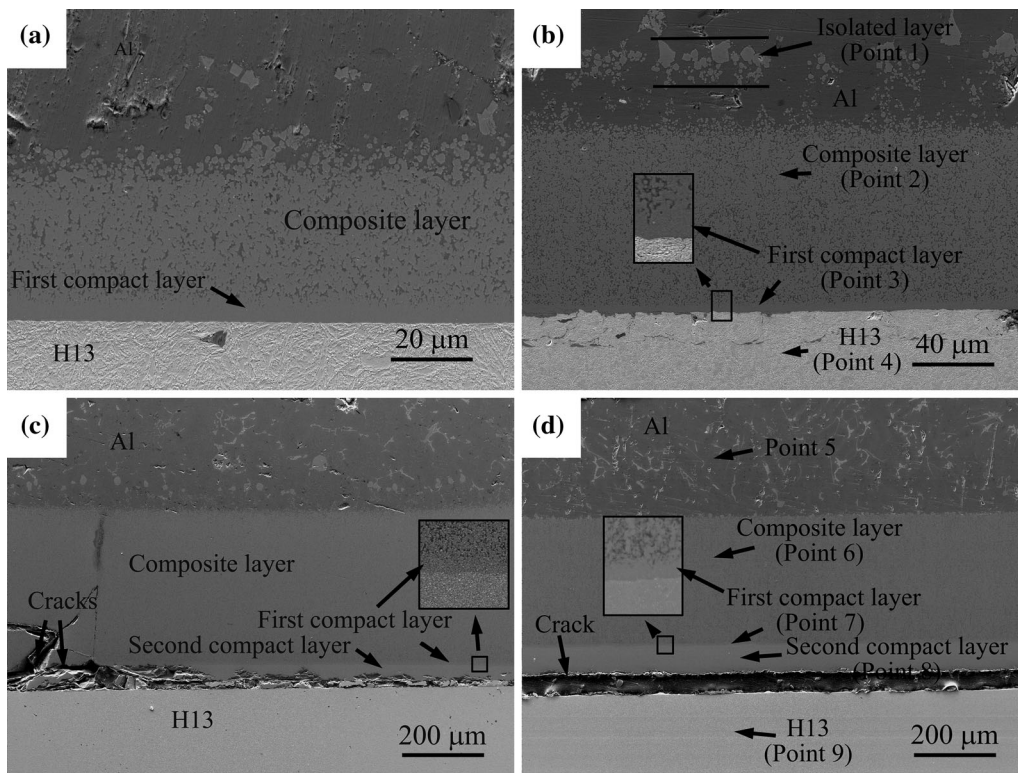


Fig. 1—SE images of typical stationary diffusion layer after (a) 1/8 h, (b) 8 h, (c) 8 h, and (d) 16 h stationary immersion.

Table I. EDX Elemental Distribution of Different Layers in Fig. 1(b) and (d)

	Cr (wt pct/at. pct)	Al (wt pct/at. pct)	Si (wt pct/at. pct)	Fe (wt pct/at. pct)	(wt pct/at. pct)
Point 1	4.15/2.55	60.32/71.55	9.77/11.13	25.76/14.76	
Point 2	4.62/2.81	63.47/74.45	8.57/9.66	21.21/12.02	Cu 2.13/1.06
Point 3	2.82/1.76	56.39/67.64	12.16/14.01	28.62/16.59	
Point 4	5.50/5.76	0.49/0.99	1.49/2.89	91.23/88.97	V 1.3/1.39
Point 5		82.39/87.73	6.31/6.45	11.3/5.81	
Point 6	5.04/3.02	64.66/74.62	9.92/11.00	20.38/11.36	
Point 7	2.98/1.87	55.53/66.98	12.10/14.02	29.40/17.13	
Point 8	3.43/2.34	50.39/66.34	3.08/3.9	43.10/27.42	
Point 9	5.96/6.37			94.04/93.63	

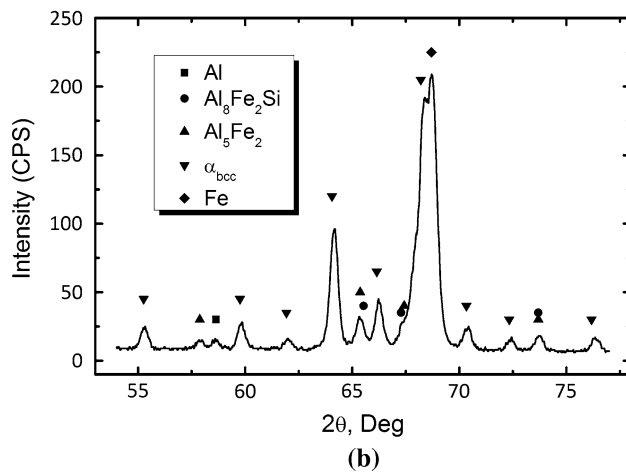
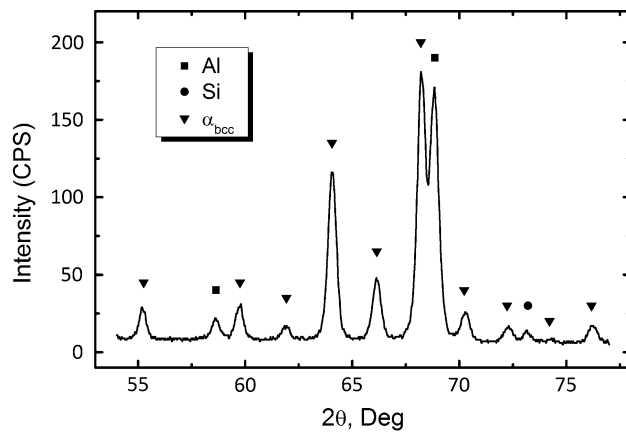


Fig. 2—Comparison of XRD patterns of (a) composite layer, (b) composite layer, two compact layers, and H13 tool steel matrix after 64 h stationary immersion.

were taken from the sample with 64 hours immersion time due to the very wide composite layer and compact layers (Figure 5(c)). A scanning electron microscope (SEM) equipped with an EDS and optical microscopy were used to analyze the intermetallic layers. Samples were prepared through mounting, grinding and polishing. Subsequently, the samples were etched using nital (4 pct nitric acid and 96 pct ethanol) at room temperature with an immersion time of 30 seconds to reveal A380 aluminum alloy, soldering product, and H13 matrix.

III. RESULTS AND DISCUSSION

Typical SEM images of diffusion layers with four different diffusion durations are presented in Figure 1. All samples have a composite layer including an Al-Fe reaction phase, a Fe-rich Al layer, and a Si layer in between. Adjacent to the composite layer, a thin compact layer of a relatively constant thickness was observed in all samples. However, samples with longer diffusion times (8 hours or longer) have a second compact layer, which is located between the first compact layer and H13 matrix, see Figures 1(c) and (d). Different layers are separated by flat interfaces. The detachment of reaction layers from H13 tool steel was observed. In addition, cracks are present in the second compact layer with a tendency to propagate into the other reaction layers (Figures 1(c) and (d)). The detachment and cracking can be attributed to one or the combination of the following factors: brittle reaction layers, quench process, and/or different thermal and mechanical properties of the different layers.

Table I shows the results of elemental distribution in different layers using EDX analysis. The weight percentage of Fe element increases from aluminum alloy side to H13 tool steel side, while the percentage of Al element shows an opposite trend. However, the percentage of Si element increases to its peak value at the first compact layer and then drop to nearly zero. It was apparent that composite layer and isolated layer have similar composition. The results indicate that isolate layer is formed from the detachment of composite layer.

Figures 2(a) and (b) show the XRD spectra of composite layer and all layers together, respectively. There are three phases in the composite layer: α_{bcc} , Si, and Al phases.^[1] According to the EDX result, α_{bcc} is made of Al, Fe, Si, and other minor elements. From the results of EDX and XRD pattern in Figure 2(b), the first compact layer can be identified as Al_8Fe_2Si and the second compact layer can be identified as Al_3Fe_2 .

The growth of each individual intermetallic layer with immersion time is shown in Figure 3 and can be described by the following equations in general:

$$Y = Kt + c \text{ (linear law),} \quad [1]$$

$$Y = Kt^{1/2} + c \text{ (parabolic law),} \quad [2]$$

where Y is the thickness of an intermetallic layer (μm), K is the growth constant ($\mu\text{m}/\text{hour}$ for Eq. [1] and $\mu\text{m}/$

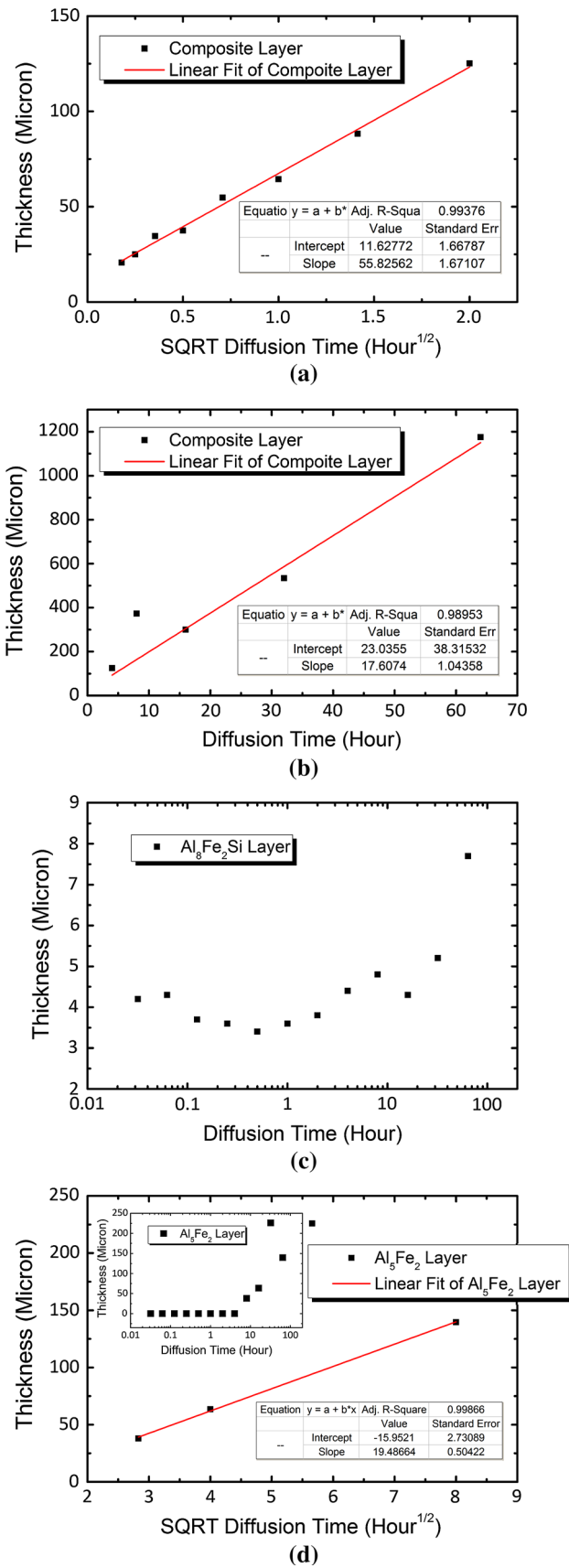


Fig. 3—Thickness of intermetallic layers vs stationary diffusion time (a, b) composite layer, (c) $\text{Al}_8\text{Fe}_2\text{Si}$ layer, and (d) Al_5Fe_2 layer.

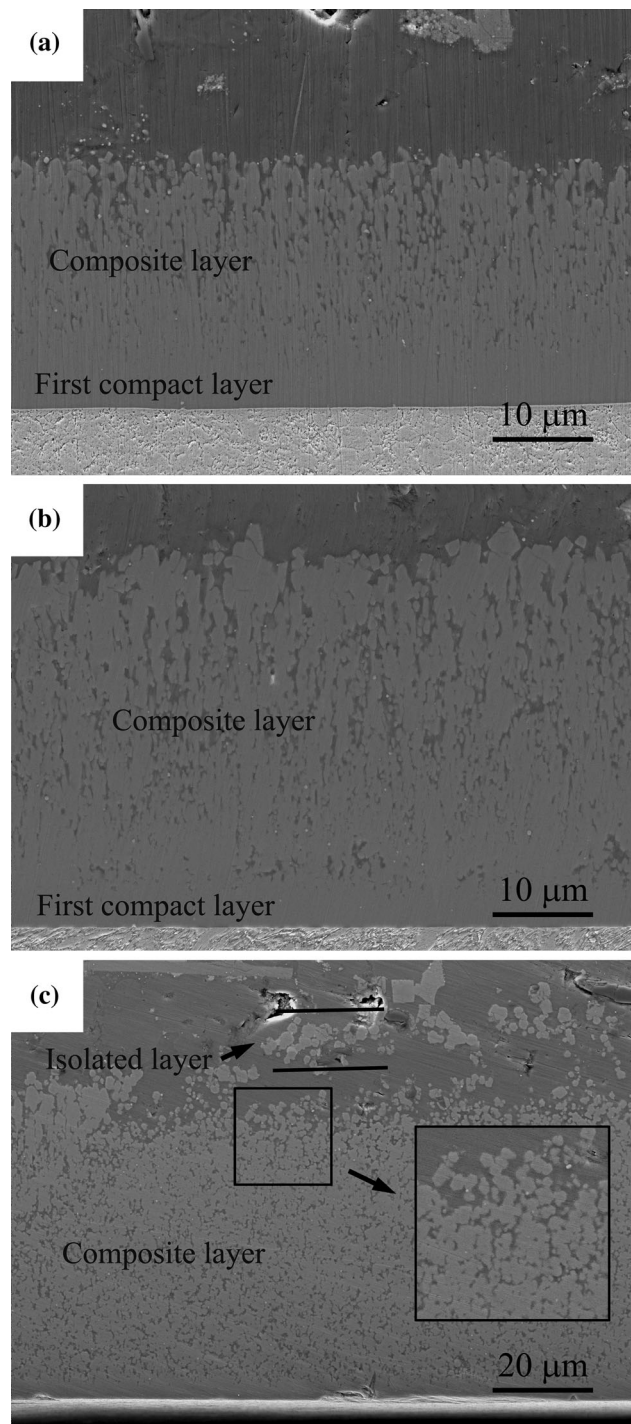


Fig. 4—Morphology changes of composite layer from rod to spherical shape (a) rod-like shape, (b) combined shape, and (c) spherical shape.

hour^{1/2} for Eq. [2]), t is the immersion time (hour), and c is a constant of the equation (μm). The parabolic law describes that growth governed by interdiffusion of chemical reaction species, while the linear law describes the growth dominated by chemical reactions at an interface.^[5,12] The growth rate of a composite layer exhibits a transition from power exponent to

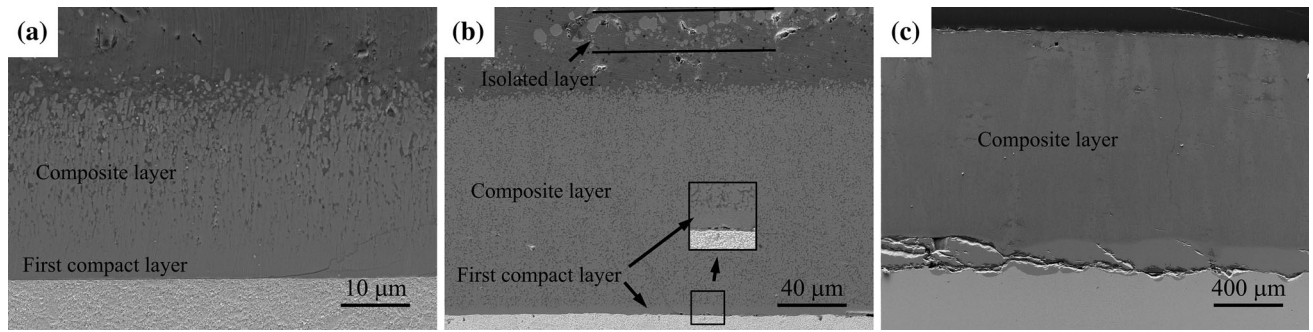


Fig. 5—Evolution of an isolate composite layer with immersion time (a) 113 s, (b) 4 h, and (c) 64 h.

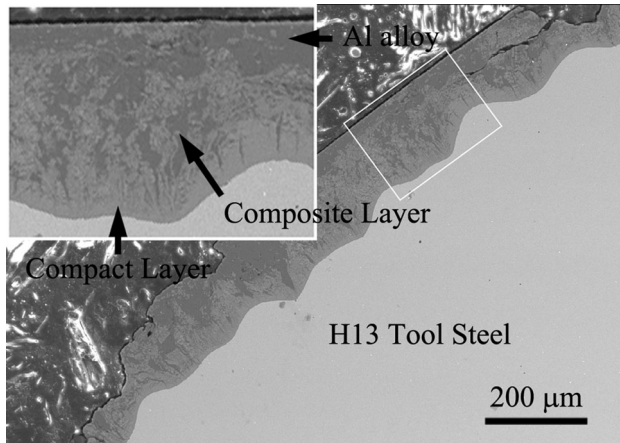


Fig. 6—Soldering (diffusion layers) formed on a core pin in real HPDC process.

linear manner with diffusion time at 4 hours of immersion time in Figures 3(a) and (b) (excluding odd data for 8 hours immersion time). The thickness of $\text{Al}_8\text{Fe}_2\text{Si}$ compact layer changes little with increasing immersion time. And the thickness range is from 3 to 8 μm , which is much thinner than composite layer or Al_5Fe_2 compact layer. The Al_5Fe_2 compact layer does not appear until the immersion time reaches 8 hours. The thickness increase of this layer follows a parabolic relation with diffusion time (excluding odd data for 32 hours). The relation between thickness of each layer and immersion time can be expressed as Eqs. [3] to [5]:

$$Y_{C1} = 55.83t^{1/2} + 11.63, \quad [3]$$

$$Y_{C2} = 17.61t + 23.04, \quad [4]$$

$$Y_{\text{Al}_5\text{Fe}_2} = 19.47t^{1/2} - 15.95, \quad [5]$$

where Y_{C1} is the thickness of composite layer with immersion time less than 4 hours (μm), Y_{C2} is the thickness of composite layer with immersion time greater than 4 hours (μm), and $Y_{\text{Al}_5\text{Fe}_2}$ is the thickness of Al_5Fe_2 layer (μm).

The morphology of intermetallic phase in the composite layer changes from a rod to spherical shape when immersion time increases, as shown in Figure 4. The

rod-like α_{bcc} phase starts to join together and grow larger between 0.0625 and 0.25 hours of immersion time. The rod-like α_{bcc} phase changes to spherical shape at half an hour of immersion time. The shape change also influences the size of α_{bcc} phase greatly, which becomes smaller compared to the previous microstructure. The individual particle size ranges from sub-micron to about 2 μm . Several large irregular particles are made of small particles.

Figure 5 shows an isolated layer about 50 μm away from the composite layer in samples with immersion time between 0.125 and 8 hours (Figures 1(b), 4(c), and 5(b)). This layer consists of large α_{bcc} particles, which is the same particles in the composite layer, indicating that the particles in the isolate layer are originated from particles in the composite layer. Coalescence of small individual particles is favored thermodynamically under the testing conditions. No isolate layer is found in this study for an immersion time less than 0.0625 hour (Figure 5(a)) and longer than 16 hours (Figure 5(c)).

Reaction layers of H13 tool steel core pin and A380 aluminum alloy in real HPDC are shown in Figure 6. The outside layer is solidified aluminum alloy, followed by a mushy layer adjacent to a compact layer. These characteristics are similar to the stationary immersion results at short diffusion time. There is a wavy interface between H13 tool steel and the compact layer. The total thickness of reaction layers was about 150 μm , similar to the thickness of the 4 hours stationary immersion. From previous results, the compact and composite layers are made of $\text{Al}_8\text{Fe}_2\text{Si}$ phase and the mixture of α_{bcc} , Al, and Si phases, respectively.^[1,19]

Figure 7 shows a schematic plot of existing phases in each layer with immersion time. In this study, an $\text{Al}_8\text{Fe}_2\text{Si}$ layer and a composite layer in rod shape were observed after a very short immersion time. Then, the composite layer changed to spherical particles after about 0.0625 hour, and an isolated layer began to form near the outside of the composite layer. When immersion time increased to 4 hours, an Al_5Fe_2 layer was produced. Shortly after the appearance of Al_5Fe_2 phase (“exist” in Figure 7), the isolate layer disappeared.

The formation of a composite layer and the first compact layer provides an evidence that $\text{Al}_8\text{Fe}_2\text{Si}$ and α_{bcc} form readily when H13 steel is brought into contact with A380. In contrast to the stationary immersion test, it is difficult for the second compact layer to forms in a

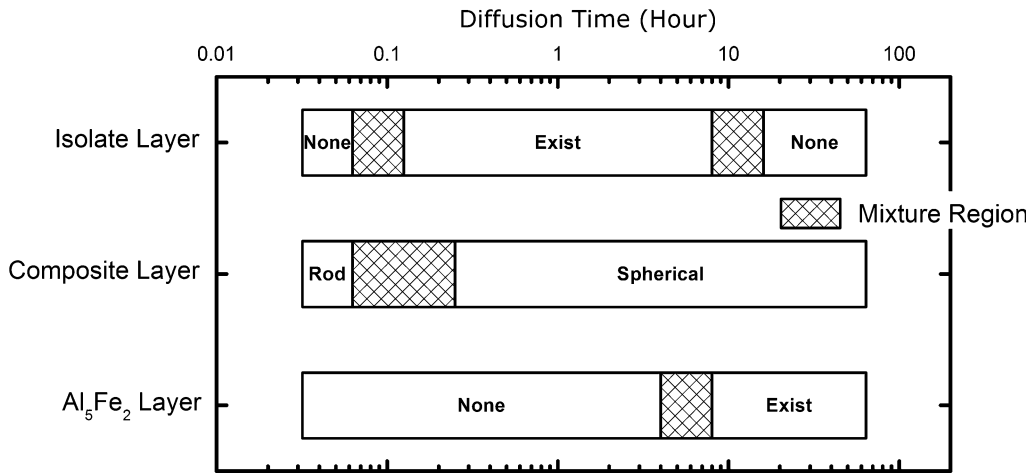


Fig. 7—Schematic presenting the three key phenomena during the stationary immersion.

real HPDC process. The change of growth laws is a result of the formation of an Al_5Fe_2 layer due to the orthorhombic crystal structure of Al_5Fe_2 , which contains 30 pct voids in the $\langle c \rangle$ direction, accelerating the diffusion of Al atoms into the reaction front.^[3]

The formation of an isolate layer can be realized by repeating the following three steps: (1) the formation of particles in the composite layer; (2) the coalescence of large particles; and (3) the transport of large particles into molten aluminum. The formation of the second compact layer affects the formation of the isolated layer by changing the distribution of Fe and Al in the reaction products. The consumption of Al and Fe elements by forming Al_5Fe_2 retards the formation of the isolate layer.

The growth of spherical particles and the rod-like phase from the first compact layer are governed by different growth mechanisms of the composite layer. It can also be elucidated from the fact that the rod-like phase grows from the compact layer, and at the same time, the bonding strength between the composite layer and the compact layer is high. As a result, an isolated layer can hardly form at the same time.

Reaction products in HPDC core pins show the difficulties of an Al_5Fe_2 phase formation, which could be attributed to the rapid flow of molten aluminum alloy that brings in new alloy melt, peels off the composite layer, and takes it away. As a result, only readily formed layers are observed on the surface of the core pins after soldering.

IV. CONCLUSION

Three intermetallic layers form on H13 tool steel successively with increasing immersion time in the stationary immersion tests. The first compact and the composite layer form readily after a very short immersion period, while the second compact layer forms after an immersion period longer than 4 hours.

The composite layer is a mixture of Al, Si, and α_{bcc} phases. The shape of α_{bcc} phase starts to change from

rods to mushy globular shape at a 0.0625 hour immersion time. The growth rate of the composite layer is controlled by the diffusion rate of related elements when the immersion time is shorter than 4 hours. Then the growth rate changes to a linear type due to the formation of the second compact layer. The first compact layer forms at the beginning of the reaction between A380 alloy and H13 steel, maintaining a constant thickness through a dynamic equilibrium between formation and decomposition. The second compact layer forms after 4 hours of immersion time and grows parabolically with immersion time. This layer is a binary compound layer, the repelled elements other than Al and Fe may form barriers for the diffusion of Si atoms, thus speeding up the growth of the composite layer.

Unlike the stationary immersion test, reaction of core pins with A380 alloy in a real HPDC process produces only two reaction layers: the composite layer and the first compact layer. The rapid flow of molten aluminum alloy and fresh molten alloy in each die casting cycle flushes the composite layer away. Therefore, the thickness of the reaction layer in real die casting maintains around $150 \mu\text{m}$, and the formation of the second compact layer is not favored.

ACKNOWLEDGMENTS

The authors acknowledge the support of North American Die Casting Association.

REFERENCES

1. Z.W. Chen, D.T. Fraser, and M.Z. Jahedi: *Mater. Sci. Eng. A*, 1999, vol. 260, pp. 188–96.
2. K.A. Nazari and S.G. Shabestari: *J. Alloys Compd.*, 2009, vol. 478, pp. 523–30.
3. T.-S. Shih and S.-H. Tu: *Mater. Sci. Eng. A*, 2007, vols. 454–455, pp. 349–56.
4. A. Bouayad, C. Gerometta, A. Belkebir, and A. Ambari: *Mater. Sci. Eng. A Struct.*, 2003, vol. 363, pp. 53–61.

5. K. Bouche, F. Barbier, and A. Coulet: *Mater. Sci. Eng. A Struct.*, 1998, vol. 249, pp. 167–75.
6. S. Kobayashi and T. Yakou: *Mater. Sci. Eng. A*, 2002, vol. 338, pp. 44–53.
7. Y. Tanaka and M. Kajihara: *Mater. Trans.*, 2009, vol. 50, pp. 2212–20.
8. V.N. Yeremenko, Y.V. Natanzon, and V.I. Dybkov: *J. Mater. Sci.*, 1981, vol. 16, pp. 1748–56.
9. W.J. Cheng and C.J. Wang: *Surf. Coat. Technol.*, 2009, vol. 204, pp. 824–28.
10. A. Coulet, K. Bouche, F. Marinelli, and F. Barbier: *J. Appl. Phys.*, 1997, vol. 82, pp. 6001–07.
11. V.I. Dybkov: *J. Mater. Sci.*, 1986, vol. 21, pp. 3085–90.
12. V.I. Dybkov: *J. Mater. Sci.*, 1986, vol. 21, pp. 3078–84.
13. G. Eggeler, W. Auer, and H. Kaesche: *J. Mater. Sci.*, 1986, vol. 21, pp. 3348–50.
14. G.V. Kidson: *J. Nucl. Mater.*, 1961, vol. 3, pp. 21–29.
15. J.E. Nicholls: *Anti Corros. Methods Mater.*, 1964, vol. 11, pp. 16–21.
16. G. Pasche, M. Scheel, R. Schäublin, C. Hébert, M. Rappaz, and A. Hessler-Wyser: *Metall. Mater. Trans. A*, 2013, vol. 44A, pp. 4119–23.
17. S.R. Shatynski, J.P. Hirth, and R.A. Rapp: *Acta Metall.*, 1976, vol. 24, pp. 1071–78.
18. S. Shankar and D. Apelian: *Metall. Mater. Trans. B*, 2002, vol. 33B, pp. 465–76.
19. J. Song, T. DenOuden, and Q. Han: *Metall. Mater. Trans. A*, 2012, vol. 43A, pp. 415–21.
20. S. Shankar and D. Apelian: *JOM*, 2002, vol. 54, pp. 47–54.